# The Science and Technology of Carbon Nanotubes

Edited by

Kazuyoshi Tanaka
*Kyoto University, Japan*

Tokio Yamabe
*Kyoto University, Japan*

Kenichi Fukui †
*Institute for Fundamental Chemistry, Japan*

1999
Elsevier
Amsterdam - Lausanne - New York - Oxford - Shannon - Singapore - Tokyo

ELSEVIER SCIENCE Ltd
The Boulevard, Langford Lane
Kidlington, Oxford OX5 1GB, UK



First edition 1999

Library of Congress Cataloging in Publication Data
A catalog record from the Library of Congress has been applied for.

British Library Cataloguing in Publication Data
A catalogue record from the British Library has been applied for.

ISBN: 0 08 042696 4

♾ The paper used in this publication meets the requirements of ANSI/NISO Z39.48-1992 (Permanence of Paper).
Printed in The Netherlands.

CHAPTER 7

# Behaviour of Single-Walled Carbon Nanotubes in Magnetic Fields

HIROSHI AJIKI[1] and TSUNEYA ANDO[2]

[1]*Department of Physical Science, Graduate School of Engineering Science, Osaka University 1-3 Machikaneyama Toyonaka 560-8531, Japan*
[2]*Institute for Solid State Physics, University of Tokyo 7-22-1 Roppongi, Minato-ku, Tokyo 106-8666, Japan*

*A brief review is given on electronic properties of carbon nanotubes, in particular those in magnetic fields, mainly from a theoretical point of view. The topics include a giant Aharonov-Bohm effect on the band gap and optical absorption spectra, a magnetic-field induced lattice distortion and a magnetisation and susceptibility of ensembles, calculated based on a* **k•p** *scheme.*

## 1 Introduction

A carbon nanotube (CNT) can be either a metal or semiconductor depending on their diameters and helical arrangement when we ignore effect of curvature, which causes hybridisation of $\pi$- and $\sigma$-orbital for a CNT with extremely small diameter [1]. This result was first predicted by means of a tight-binding model [2] and can be well reproduced in a **k•p** method [3]. In this chapter we give electronic properties of a single-walled CNT (SWCNT) in magnetic fields with use of the **k•p** method.

The **k•p** method provides analytic descriptions on electronic states of CNT. It shows, for example, that the band gap of a semiconducting CNT is inversely proportional to the diameter because of a linear dispersion of the bands. It is suitable also for descriptions of the electronic motion in external perturbations such as electric and magnetic fields.

In Sec. 2 the effective mass equation is introduced and the band structure is discussed with a special emphasis on an Aharonov-Bohm effect. Optical absorption spectra are discussed in Sec. 3. A lattice instability, in particular induced by a magnetic field perpendicular to the tube axis, is discussed in Sec. 4 and magnetic properties of ensembles of CNTs are discussed in Sec. 5.

## 2 Aharonov-Bohm Effect

A CNT is specified by a chiral vector $\mathbf{L} = n_a\mathbf{a} + n_b\mathbf{b}$ with integer $n_a$ and $n_b$ and basis vectors **a** and **b** ($|\mathbf{a}| = |\mathbf{b}| = a = 2.46$ Å) as is shown in Fig. 1. In the ($x'$, $y'$) system of coordinates fixed onto a graphite sheet, we have $\mathbf{a} = (a, 0)$ and $\mathbf{b} = (-a/2, \sqrt{3}a/2)$. We introduce another coordinate system on CNTs, where the $x$ and $y$ directions are along the circumference and the axis, respectively.
A graphite sheet is a zero-gap semiconductor in the sense that the conduction and valence bands consisting of $\pi$-states touch at K and K' points of the Brillouin zone, whose wave vectors are given by $\mathbf{K} = (2\pi/a)(1/3, 1/\sqrt{3})$ and $\mathbf{K}' = (2\pi/a)(2/3, 0)$. The unit cell has an area $\sqrt{3}a^2/2$ and contains two carbon atoms (denoted as A and B) as shown in Fig. 1.

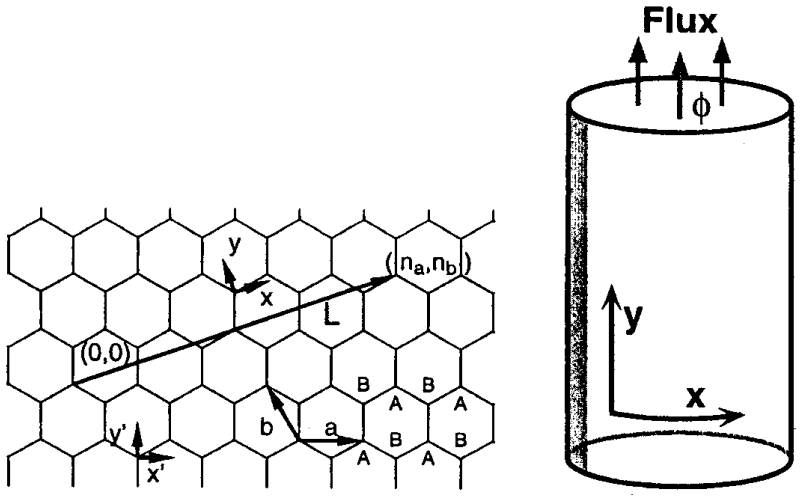


**Fig. 1.** A single layer of graphite and a CNT in a magnetic flux passing through its cross section.

Electronic states (with an appropriate choice of phases of the Bloch functions) near K and K' points of two-dimensional (2D) graphite are described by the **k•p** equation:

$$\gamma(\sigma_x k_x + \sigma_y k_y)F_K(\mathbf{r}) = \varepsilon(\mathbf{k})F_K(\mathbf{r}),$$

$$\gamma(\sigma_x k_x - \sigma_y k_y)F_{K'}(\mathbf{r}) = \varepsilon(\mathbf{k})F_{K'}(\mathbf{r}), \qquad (1)$$

where $\gamma$ is the band parameter, $\mathbf{k} = (k_x, k_y)$ is a wave-vector operator, and $\sigma_x$, $\sigma_y$ and $\sigma_z$ are the Pauli spin matrices. In the above equations, the envelope functions are written as

$$F_K(\mathbf{r}) = \begin{pmatrix} F_K^A(\mathbf{r}) \\ F_K^B(\mathbf{r}) \end{pmatrix}, \quad F_{K'}(\mathbf{r}) = \begin{pmatrix} F_{K'}^A(\mathbf{r}) \\ F_{K'}^B(\mathbf{r}) \end{pmatrix}. \qquad (2)$$

Eq.(1) has the form of Weyl's equation for massless neutrinos.

Electronic states of CNTs with sufficiently large diameter can be obtained by imposing the generalised periodic boundary condition in the circumference direction, $\Psi(\mathbf{r} + \mathbf{L}) = \Psi(\mathbf{r})\exp(2\pi i\varphi)$, with $\varphi = \phi/\phi_0$, where $\phi$ is an Aharonov-Bohm (AB) magnetic flux passing through the cross section of CNT and $\phi_0 = hc/e$ is the magnetic flux quantum. The Bloch functions at the K and K' points change their phase by $\exp(2\pi i\nu/3)$ and $\exp(-2\pi i\nu/3)$, respectively, where $\nu$ is an integer defined by $n_a + n_b = 3M + \nu$ with integer $M$ and can take 0 and $\pm 1$. This phase change should be cancelled by that of the envelope functions and the boundary condition for the envelope function associated with the K point is given by

$$F_K(\mathbf{r} + \mathbf{L}) = F_K(\mathbf{r}) \exp\left[2\pi i\left(\varphi - \frac{\nu}{3}\right)\right], \tag{3}$$

At the K' point, $\nu$ should be replaced by $-\nu$ in this equation.
Energy levels in CNT are obtained by putting $k_x = \kappa_{\nu\varphi}(n)$ and $k_y = k$ in the above **k•p** equation as [3]

$$\varepsilon_{\nu\varphi}^{(\pm)}(n, k) = \pm\gamma\sqrt{\kappa_{\nu\varphi}(n)^2 + k^2}, \quad \kappa_{\nu\varphi}(n) = \frac{2\pi}{L}\left(n + \varphi - \frac{\nu}{3}\right), \tag{4}$$

where $n$ is an integer and the upper (+) and lower (−) signs represent the conduction and valence bands, respectively. In the absence of a magnetic flux, $\varphi = 0$, CNT becomes metallic for $\nu = 0$ and semiconducting with gap $E_g = 4\pi\gamma/3L$ for $\nu = \pm 1$. Figure 2 compares this gap to that obtained in a tight-binding model [4].

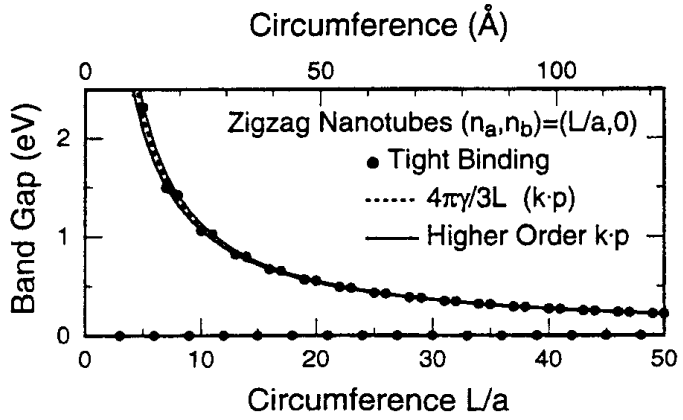


**Fig. 2.** Energy gap of monolayer CNTs specified by $(n_a, n_b)=(m, 0)$. The dots are calculated in a tight-binding model and the dotted line represents $4\pi\gamma/3L$ given in the **k•p** scheme. The solid lines are the results of a higher order **k•p** scheme. Use has been made of $\gamma$=6.46 eV Å.

In the presence of a magnetic flux, the boundary condition is changed by the Aharonov-Bohm effect and the band gap exhibits an oscillation between 0 and $2\pi\gamma/L$ with period $\phi_0$ as is shown in Fig. 3.

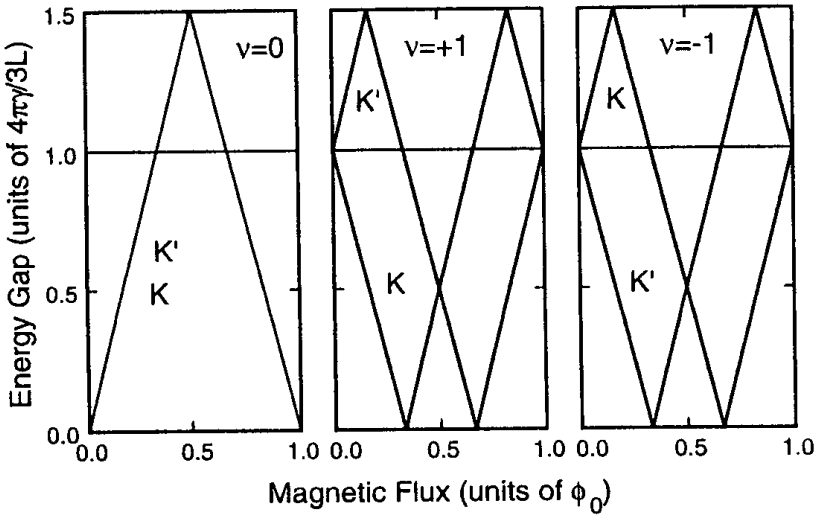


**Fig. 3.** Energy gap versus magnetic flux passing through the tube cross section for metallic (ν=0) and semiconducting (ν=±1) CNT.

In the presence of a magnetic field $H$ perpendicular to the tube axis, the effective field for electrons in a CNT is given by $H(x) = H\cos(2\pi x/L)$ which is periodic in the circumference direction. The parameter characterising its magnitude is given by $(L/2\pi l)^2$, where $l = \sqrt{c\hbar/eH}$ is the magnetic length or the radius of the smallest cyclotron orbit. In the case $(L/2\pi l)^2 << 1$, the field can be regarded as a small perturbation, while in the case $(L/2\pi l)^2 >> 1$, Landau levels are formed on the cylinder surface.

**Table 1.** Typical magnetic fields (T) for CNTs with different circumferences. At the field corresponding to $\phi = \phi_0$ the total magnetic flux passing through the cross section is equal to the flux quantum and at $(L/2\pi l)^2 = 1$ the magnetic length is equal to the diameter of CNT.

| Circumference (Å) | | 50 | 100 | 200 | 400 | 800 |
|---|---|---|---|---|---|---|
| Diameter (Å) | | 16 | 32 | 64 | 127 | 255 |
| Gap (meV) | | 541 | 270 | 135 | 68 | 34 |
| Magnetic field (T) | $\phi = \phi_0$ | 2080 | 520 | 130 | 32 | 8 |
| | $(L/2\pi l)^2 = 1$ | 1040 | 260 | 65 | 16 | 4 |

An interesting feature of Weyl's equation lies in the fact that Landau levels are formed at energy $\varepsilon = 0$. This has long been known as the origin of a large diamagnetism of graphite. Figure 4 gives some examples of energy bands of a metallic and semiconducting CNT in perpendicular magnetic fields, which clearly shows the formation of flat Landau levels at the Fermi level in high fields. Note that there is no difference in the spectra between metallic ($\nu = 0$) and semiconducting ($\nu = \pm 1$) CNTs for $(L/2\pi l)^2 >> 1$. This comes from the fact that the wave function is localised in the circumference direction and the boundary condition becomes irrelevant. Thus in high field the energy bands become

independent of an AB flux also. Table 1 gives typical magnetic fields as a function of the circumference and diameter of CNT.

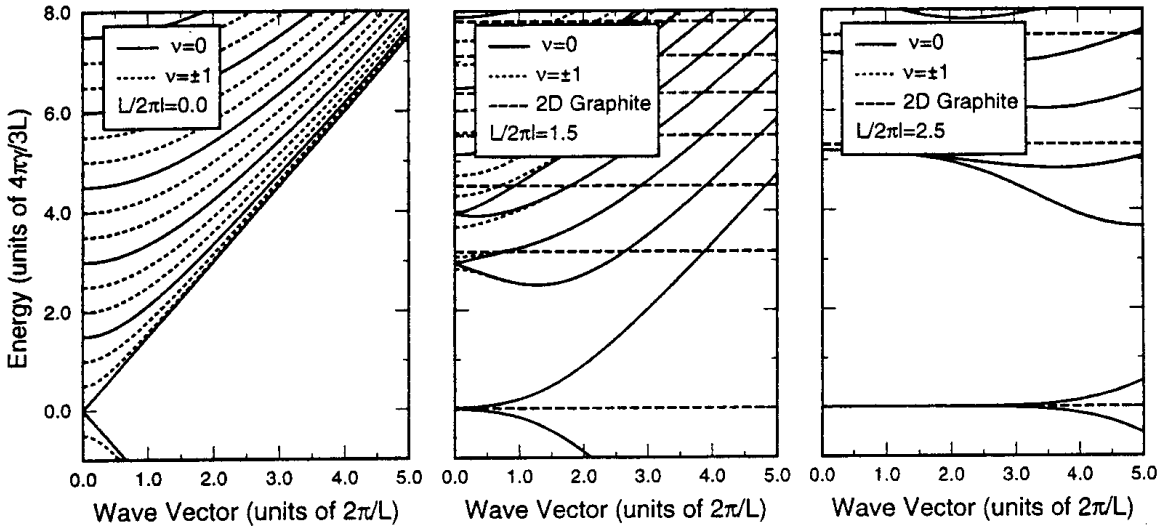


**Fig. 4.** Some examples of calculated energy bands of a metallic CNT in magnetic fields perpendicular to the axis.

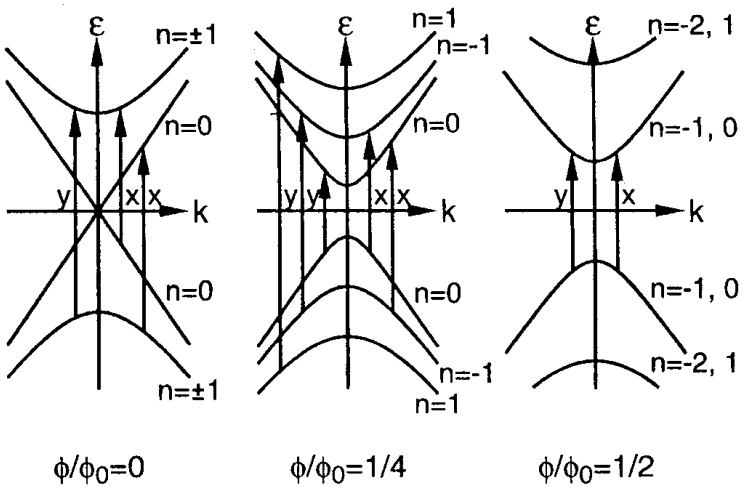


**Fig. 5.** Energy bands of a metallic CNT in the presence of a magnetic flux and allowed optical transitions for the $x$ and $y$ polarisations.

## 3 Optical Absorption

In the optical absorption, two different polarisations of light should be considered: the electric field is along (parallel or $y$ polarisation) and perpendicular (perpendicular or $x$) to the axis. Figure 5 shows the energy band of a metallic CNT for flux $\phi/\phi_0 = 0$, 1/4 and 1/2 and the process of optical transitions for the parallel and perpendicular polarisations. Some examples of calculated absorption

spectra of semiconducting CNTs in a magnetic flux are given in Fig. 6 [5]. For parallel polarisation, the spectrum changes dramatically as a function of the magnetic flux due to the AB effect. In the case of the perpendicular polarisation, on the other hand, the incident electric field induces a large polarisation of CNT, which suppresses the absorption almost completely.

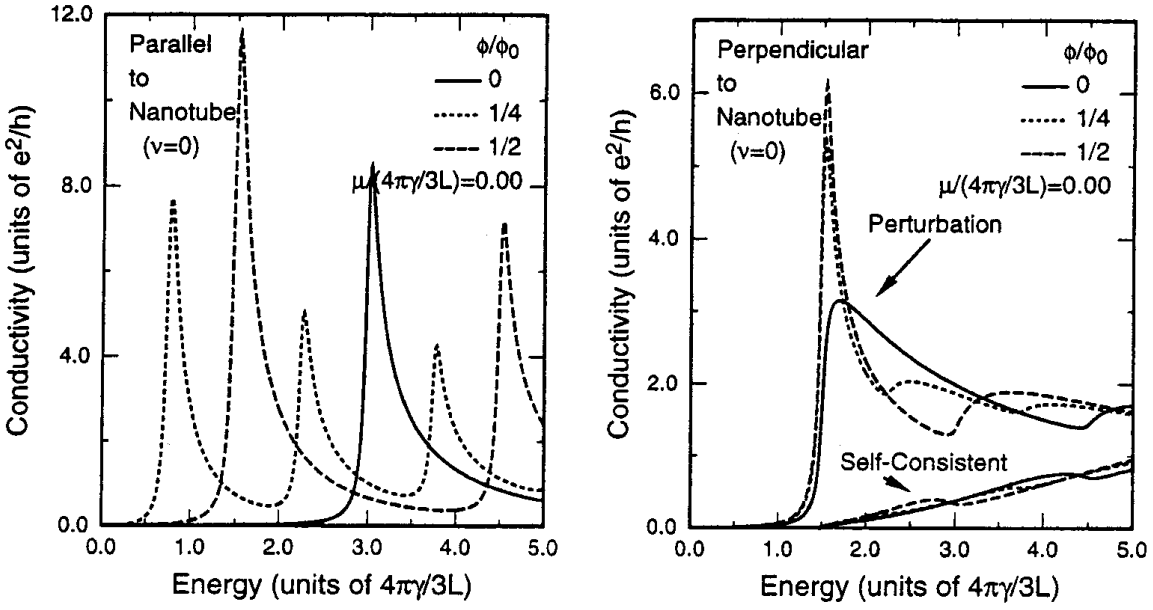


**Fig. 6.** Calculated optical absorption spectra of a metallic CNT in a magnetic flux. In the case that the electric field is parallel to the axis (left), the absorption exhibits a distinct AB effect. In the case of the perpendicular polarisation (right) the depolarisation effect suppresses the absorption almost completely.

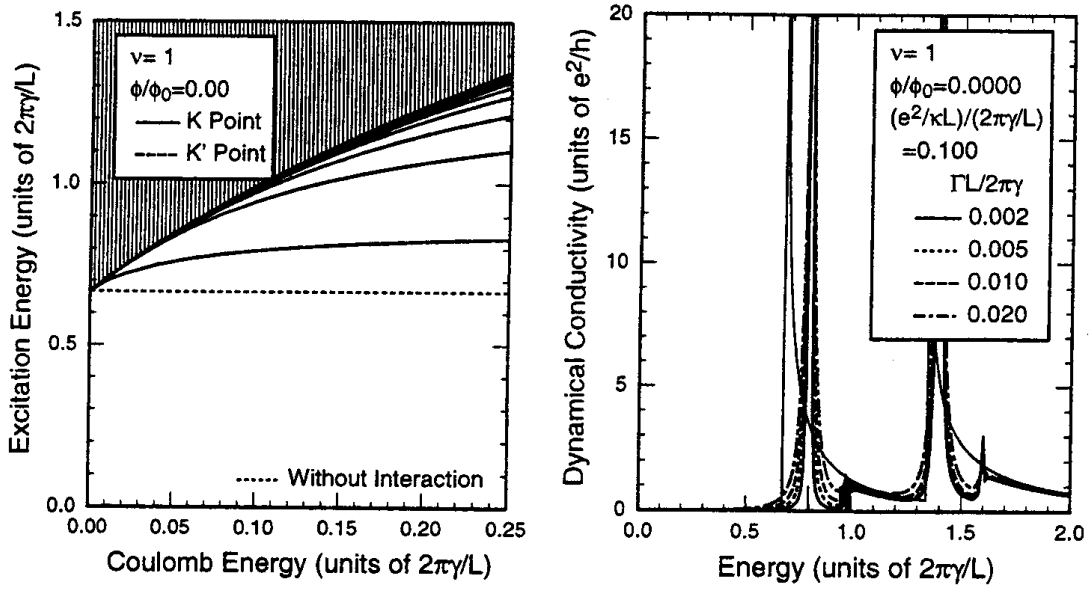


**Fig. 7.** Calculated optical excitation spectra (left) and exciton absorption spectra (right) of a semiconducting CNT for a parallel polarisation.

It is well known that the exciton binding energy becomes infinite in the limit of an ideal one-dimensional (1D) electron-hole system [6,7]. This is the origin of the large enhancement of the oscillator strength of the 1D exciton. Figure 7 gives some examples of optical excitation and absorption calculated in a conventional screened Hartree-Fock approximation used in bulk systems. It shows that the band gap is strongly enhanced by the Coulomb interaction and the exciton bound states lie at energies slightly higher than the band gap in the absence of the Coulomb interaction and that considerable optical intensity is transferred to the lowest exciton bound states.

## 4 Lattice Distortion

It is known that a metallic 1D system is unstable against lattice distortion and turns into an insulator. In CNTs instabilities associated two kinds of distortions are possible, in-plane and out-of-plane distortions as shown in Fig. 8. The in-plane or Kekulé distortion has the form that the hexagon network has alternating short and long bonds ($-u_1$ and $2u_1$, respectively) like in the classical benzene molecule [8,9,10]. Due to the distortion the first Brillouin zone reduces to one-third of the original one and both K and K' points are folded onto the $\Gamma$ point in a new Brillouin zone. For an out-of-plane distortion the sites A and B are displaced up and down ($\pm u_2$) with respect to the cylindrical surface [11]. Because of a finite curvature of a CNT the mirror symmetry about its surface are broken and thus the energy of sites A and B shift in the opposite direction.

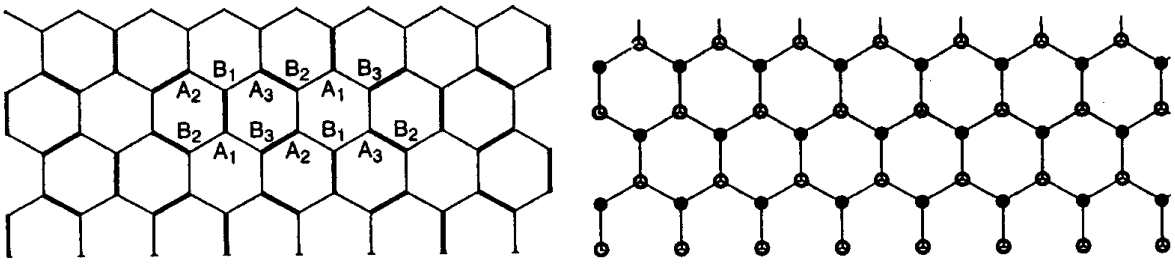


**Fig. 8.** Lattice distortions in a graphite sheet. For an in-plane distortion (left), the bond denoted by a thin line becomes shorter and that denoted by a thick line becomes longer, leading to a unit cell three times as large as the original. For an out-of-plane distortion (right), an atom denoted by a black dot is shifted down and that denoted by a white circle moves up.

In the presence of lattice distortions, the **k•p** equation is given by the 4×4 matrix equation given by

$$\begin{pmatrix} \gamma\left(\sigma_x k_x + \sigma_y k_y\right) + \sigma_z \Delta_2 & -i\sigma_y \Delta_1 \\ i\sigma_y \Delta_1 & \gamma\left(\sigma_x k_x - \sigma_y k_y\right) + \sigma_z \Delta_2 \end{pmatrix} \begin{pmatrix} F_K(\mathbf{r}) \\ F_{K'}(\mathbf{r}) \end{pmatrix}$$

$$= \varepsilon \begin{pmatrix} F_K(\mathbf{r}) \\ F_{K'}(\mathbf{r}) \end{pmatrix}, \tag{5}$$

which is equivalent to the relativistic Dirac equation [12]. The energy bands are given by

$$\varepsilon_\varphi^{(\pm)}(n, k, \Delta_1, \Delta_2) = \pm\sqrt{\gamma^2\kappa_\varphi(n)^2 + \gamma^2 k^2 + {\Delta_1}^2 + {\Delta_2}^2}. \tag{6}$$

This shows that the gap given by $E_g = 2\sqrt{{\Delta_1}^2 + {\Delta_2}^2}$ opens up in the absence of a magnetic flux.

The gap parameters $\Delta_1$ and $\Delta_2$ are determined by the minimisation of the total energy given by

$$E = 4 \sum_{n=-\infty}^{\infty} \sum_k \varepsilon_\varphi^{(-)} g_0\left(\left|\varepsilon_\varphi^{(-)}\right|\right) + N\frac{K_1\Delta_1^2}{2f_1^2} + N\frac{K_2\Delta_2^2}{2f_2^2}, \tag{7}$$

where $\varepsilon_\varphi^{(-)}$ is the valence-band energy, $K_1$ and $K_2$ are the force constants for the in- and out-of-plane distortions, respectively, and $N$ is the total number of carbon atoms. Further, $f_1$ and $f_2$ are defined by $\Delta_1 = f_1 u_1$ and $\Delta_2 = f_2 u_2$. We have introduced a cutoff function $g_0(\varepsilon)$ in order to extract the contribution from the states in the vicinity of the top of the valence band. The results are independent of the choice of cutoff functions as long as the function decays smoothly with energy and the cutoff energy is sufficiently large.

The gap parameters are determined under the condition that the total energy becomes minimum, and it is found that two kinds of distortions cannot coexist and that a distortion having a larger effective coupling constant $\lambda = \sqrt{3}af^2/\pi K\gamma$ occurs, where $(K, f) = (K_i, f_i)$ with $i = 1$ or 2. The gap parameter is obtained as

$$E_g(\varphi) = E_g\sqrt{1 - \left(\frac{\varphi}{\varphi_0}\right)^2}, \quad \varphi_c = \frac{\phi_c}{\phi_0} = \frac{LE_g}{4\pi\gamma},$$

$$E_g = \frac{2\pi\gamma}{L}\exp\left(-\frac{L}{a\lambda} - 1 - C\right), \quad C \approx 0.1445972. \tag{8}$$

The gap parameter or lattice distortion vanishes in the critical AB flux $\phi_c$ which opens the gap as large as that due to the distortion. For $\phi = 0$, the gap decreases exponentially as a function of the circumference $L/a$. Table 2 gives some examples for an in-plane Kekulé distortion.

For out-of-plane distortion the coefficient $f_2 = \Delta_2/u_2$ is expected to be proportional to $a/L$, since $f_2$ becomes nonzero for the finite curvature. Thus, the coupling constant is proportional to $(a/L)^2$ and the gap decreases very rapidly with the diameter as $\exp[-(L/a)^3]$. It is concluded that metallic CNTs are quite

stable against lattice distortions and hold metallic properties even at low temperatures except in extremely narrow CNTs.
The situation changes drastically in the presence of a high magnetic field perpendicular to the axis. As has been discussed in Sec. 2, Landau levels without dispersion appear at the Fermi level considerably, leading to a magnetic-field induced distortion [13,14].

**Table 2.** Calculated energy gap due to an in-plane Kekulé distortion for CNTs having chiral vector $\mathbf{L}/a = (m, 2m)$. The critical magnetic flux $\varphi_c$ and the corresponding magnetic field are also shown. The coupling constant is $\lambda \approx 1.62$.

| $m$ | | 5 | 10 | 20 |
|---|---|---|---|---|
| Diameter | (Å) | $6.78\times 10^{0}$ | $1.36 \times 10^{1}$ | $2.71 \times 10^{1}$ |
| Circumference | (Å) | $2.13 \times 10^{1}$ | $4.26 \times 10^{1}$ | $8.52 \times 10^{1}$ |
| $Eg$ | (meV) | $2.38 \times 10^{0}$ | $5.68 \times 10^{-3}$ | $6.46 \times 10^{-8}$ |
| $u$ | (Å) | $6.29 \times 10^{-5}$ | $1.50 \times 10^{-7}$ | $1.71 \times 10^{-12}$ |
| $\varphi_c$ | | $7.58 \times 10^{-4}$ | $3.62 \times 10^{-6}$ | $8.23 \times 10^{-11}$ |
| $Hc$ | (T) | $8.67 \times 10^{0}$ | $1.04 \times 10^{-2}$ | $5.89 \times 10^{-8}$ |

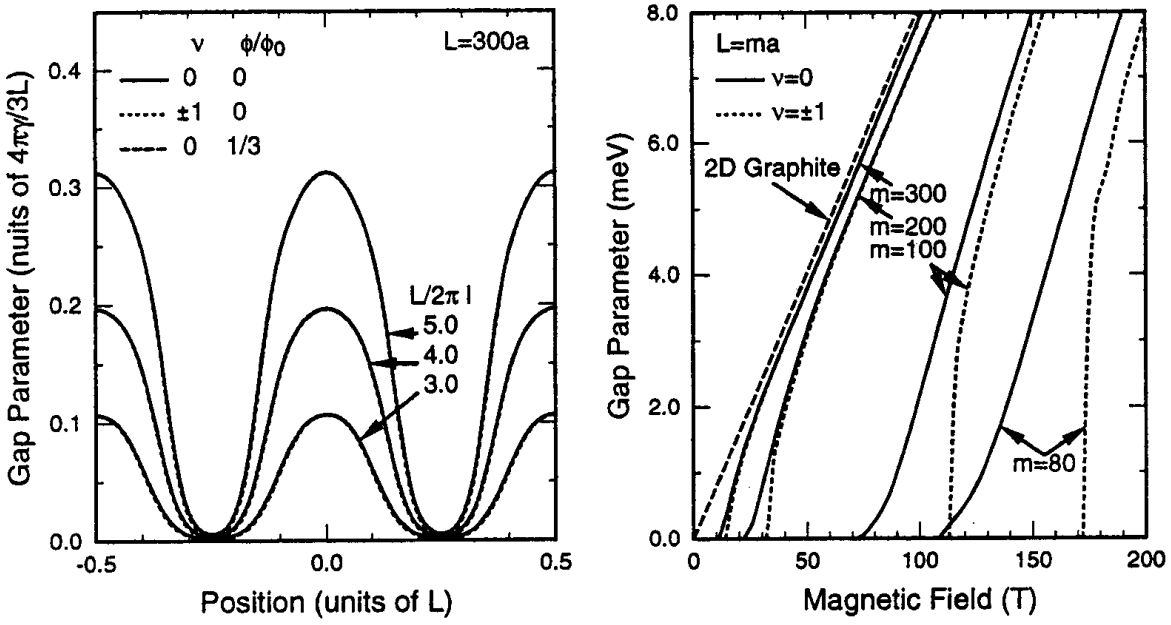


**Fig. 9.** An example of calculated in-plane lattice distortions induced by a high magnetic field (left) and the dependence of the maximum gap due to in-plane lattice distortions on a magnetic field (right).

The electron wave function becomes localised in the top and bottom part of the cylindrical surface where the effective magnetic field perpendicular to the tube surface is the largest. Thus the boundary condition along the circumference direction becomes less important in high magnetic fields as has been discussed in Sec. 2. Consequently the distinction between metallic and semiconducting

CNTs also. Further, the spatial variation of the distortion should also be considered.
The generalised **k•p** equation is the same as Eq.(5) except that the gap parameters are dependent on the position and should satisfy the boundary conditions:

$$\Delta_1(\mathbf{r}+\mathbf{L}) = \Delta_1(\mathbf{r})\exp\left(i\frac{2\pi\nu}{3}\right), \quad \Delta_2(\mathbf{r}+\mathbf{L}) = \Delta_2(\mathbf{r}). \tag{9}$$

The extra phase factor appearing in the boundary condition for $\Delta_1(\mathbf{r})$ guarantees the fact that the equations remain the same under translation $\mathbf{r} \rightarrow \mathbf{r} + \mathbf{L}$ even for $\nu = \pm 1$. Some examples of explicit numerical results for the in-plane distortion are given in Fig. 9. The figures clearly show that the lattice distortion is induced by a magnetic field in particular for CNTs with large diameter for both metallic and semiconducting CNTs and that the maximum gap approaches that of a graphite sheet.

## 5 Magnetic Properties

For a magnetic field perpendicular to the tube axis, CNTs usually exhibit diamagnetism similar to that of graphite [16,17]. For a magnetic field parallel to the axis, on the other hand, the magnetic response of CNTs becomes completely different. Figure 10 shows an example of calculated differential susceptibility as a function of a magnetic flux passing through the cross section. The most prominent feature appears for a metallic CNT as the large paramagnetic susceptibility which diverges logarithmically. This is caused by a sudden opening up of a gap due to the AB effect.
Realistic samples contain CNTs with different layer numbers, circumferences, and orientations. If effects of small interlayer interactions are neglected, the magnetic properties of a multi-walled CNT (MWCNT) are given by those of an ensemble of single-walled CNTs (SWCNTs). The distribution function for the circumference, $\rho(L)$, is not known and therefore we shall consider following two different kinds. The first is the rectangular distribution, $\rho(L) = 1/(L_{mx} - L_{mn})$ for $L_{mn} < L < L_{mx}$, which roughly corresponds to the situation that CNTs with different circumferences are distributed equally and the average layer number of MWCNTs is independent of the circumference. In realistic samples, however, the layer number increases with the outer circumference length and the distribution becomes asymmetric. The most extreme case can be realised if we assume that the inner-most shell of a CNT is $L_{mn}$. In this case the distribution is given by a triangular form, $\rho(L) = 2(L_{mx} - L)/(L_{mx} - L_{mn})^2$ for $L_{mn} < L < L_{mx}$.
Figure 11 shows magnetisation and differential susceptibility calculated for the rectangular and triangular distribution with $L_{mn}$ = 22 Å corresponding to the finest CNT so far observed and $L_{mx}$ = 942.5 Å corresponding to the thickest CNT. The experimental result of ref. 15 is also included. The calculation can

explain the experiments qualitatively, but more detailed information on the distribution of CNTs is required for more quantitative comparison.

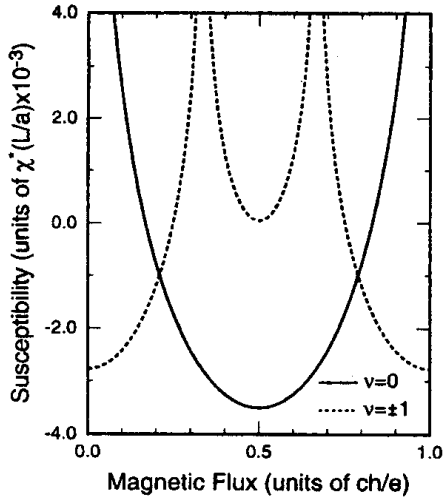


Left: **Fig. 10.** Differential susceptibilities of a CNT in the presence of a magnetic flux.

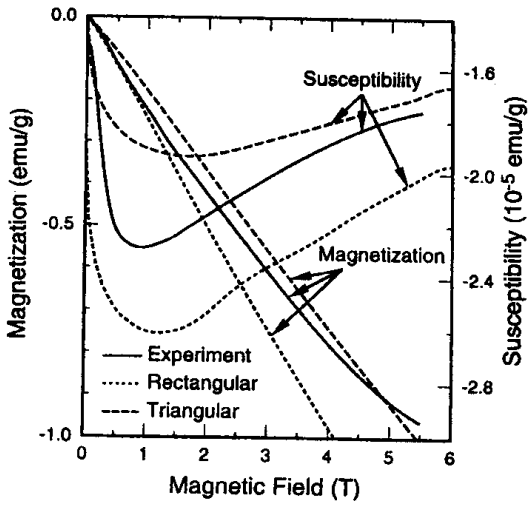


Right: **Fig. 11.** Calculated ensemble average of magnetic moment and differential susceptibility for CNTs with rectangular (dotted lines) and triangular (dashed lines) circumference distributions having $L_{mn}$=22 Å and $L_{mx}$=942.5 Å. The solid lines denote experimental results [15].

The magnetic moment is negative (diamagnetic) and its absolute value increases as a function of the magnetic field. This overall dependence is governed by that of the magnetic moment for perpendicular magnetic field and the parallel contribution or the AB effect appears as a slight deviation. This deviation becomes clearer in the differential susceptibility. In fact, the differential susceptibility increases with the decrease of the magnetic field sharply in weak magnetic fields $(L/2\pi l)^2 \lesssim 0.2$. This is a result of the divergent paramagnetic susceptibility of metallic CNTs in the parallel field, i. e., the AB effect.

## 6 Summary and Recent Developments

Electronic properties of CNTs, in particular, electronic states, optical spectra, lattice instabilities, and magnetic properties, have been discussed theoretically based on a **k•p** scheme. The motion of electrons in CNTs is described by Weyl's equation for a massless neutrino, which turns into the Dirac equation for a massive electron in the presence of lattice distortions. This leads to interesting properties of CNTs in the presence of a magnetic field including various kinds of Aharonov-Bohm effects and field-induced lattice distortions.

The same **k•p** scheme has been extended to the study of transport properties of CNTs. The conductivity calculated in the Boltzmann transport theory has shown a large positive magnetoresistance [18]. This positive magnetoresistance has been confirmed by full quantum mechanical calculations in the case that the mean free path is much larger than the circumference length [19]. When the mean free path is short, the transport is reduced to that in a 2D graphite, which has also interesting characteristic features [20].
Effects of impurity scattering in CNTs have been studied in detail and a possibility of complete absence of back scattering has been pointed out and proved rigorously except for scatterers having a potential range smaller than the lattice constant [21, 22]. This absence of back scattering disappears in magnetic fields, leading to a huge positive magnetoresistance. The conductance of an SWCNT was observed quite recently [23, 24], but experiments show large charging effects presumably due to nonideal contacts. It is highly desirable to become able to measure transport of an SWCNT with ideal Ohmic contacts.
The **k•p** scheme has been used also for the study of transport across junctions connecting tubes with different diameters through a region sandwiched by a pentagon-heptagon pair [25]. In junctions systems, the conductance was predicted to exhibit a universal power-law dependence on the ratio of the circumference of two CNTs [26]. An intriguing dependence on the magnetic-field direction was predicted also [27]. These newer topics will be discussed elsewhere.

## Acknowledgements

The authors would like to thank T. Seri, T. Nakanishi, H. Matsumura and H. Suzuura for discussion. The work is supported in part by Grant-in-Aid for Scientific Research from Ministry of Education, Science and Culture, Japan.

## References

1. Blase, X., Benedict, L. X., Shirley, E. L. and Louie, S. G., *Phys. Rev. Lett.*, 1994, **72**, 1878.
2. Hamada, N., Sawada, S. and Oshiyama, A., *Phys. Rev. Lett.*, 1992, **68**, 1579.
3. Ajiki, H. and Ando, T., *J. Phys. Soc. Jpn.*, 1993, **62**, 1255.
4. Ajiki, H. and Ando, T., *J. Phys. Soc. Jpn.*, 1996, **65**, 505.
5. Ajiki, H. and Ando, T., *Physica B*, 1994, **201**, 349; *Jpn. J. Appl. Phys. Suppl.*, 1995, **34**, 107.
6. Loudon, R., *Am. J. Phys.*, 1959, **27**, 649.
7. Elliot, R. J. and Loudon, R., *J. Phys. Chem. Solids*, 1959, **8**, 382; 1960, **15**, 196.
8. Mintmire, J. W., Dunlap, B. I. and White, C. T., *Phys. Rev. Lett.*, 1992, **68**, 631.
9. Harigaya, K., *Phys. Rev. B*, 1992, **45**, 12071.
10. Harigaya, K. and Fujita, M., *Phys. Rev. B*, 1993, **68**, 16563.
11. Saito, R., Fujita, M., Dresselhaus, G. and Dresselhaus, M. S., *Phys. Rev. B*, 1992, **46**, 1804.
12. Viet, N. A., Ajiki, H. and Ando, T., *J. Phys. Soc. Jpn.*, 1994, **63**, 3036.

13. Ajiki, H. and Ando, T., *J. Phys. Soc. Jpn.*, 1995, **64**, 260.
14. Ajiki, H. and Ando, T., *J. Phys. Soc. Jpn.*, 1996, **65**, 2976.
15. Heremans, J., Olk, C. H. and Morelli, D. T., *Phys. Rev. B*, 1994, **49**, 15112.
16. Ajiki, H. and Ando, T., *J. Phys. Soc. Jpn.*, 1998, **62**, 2470 [Errata, *J. Phys. Soc. Jpn.*, 1994, **63**, 4267].
17. Lu, J. P., *Phys. Rev. Lett.*, 1995, **74**, 1123.
18. Seri, T. and Ando, T., *J. Phys. Soc. Jpn.*, 1997, **66**, 169.
19. Ando, T. and Seri, T., *J. Phys. Soc. Jpn.*, 1997, **66**, 3558.
20. Shon, N. H. and Ando, T., *J. Phys. Soc. Jpn.*, 1998, **67**, 2421.
22. Ando, T., Nakanishi, T. and Saito, R., *J. Phys. Soc. Jpn.*, 1998, **67**, 2857.
23. Tans, S. J., Devoret, M. H., Dai, H. -J., Thess, A., Smalley, R. E., Geerligs, L. J. and Dekker, C., *Nature*, 1997, **386**, 474.
24. Bockrath, M., Cobden, D. H., McEuen, P. L., Chopra, N. G., Zettl, A., Thess, A. and Smalley, R. E., *Science*, 1997, **275**, 1922.
25. Matsumura, H. and Ando, T., *J. Phys. Soc. Jpn.*, 1998, **67**, 3542.
26. Tamura, R. and Tsukada, M., *Solid State Commun.*, 1997, **101**, 601; *Phys. Rev. B*, 1997, **55**, 4991; *Z. Phys. D*, 1997, **40**, 432.
27. Nakanishi, T. and Ando, T., *J. Phys. Soc. Jpn.*, 1997, **66**, 2973; *Physica B*, 1998, **249-251**, 136.